A Nested Primitive Equation Model for Oceanic Applications

MICHAEL A. SPALL AND WILLIAM R. HOLLAND

National Center for Atmospheric Research, Boulder, Colorado*

(Manuscript received 13 February 1990, in final form 2 July 1990)

ABSTRACT

An interactive, nested primitive equation model for oceanic applications is introduced. The model has two components that interact, which we shall call the coarse and the fine grid regions. The fine grid region is nested entirely within the domain of the coarse grid region. The interaction is achieved by an interpolation of the coarse grid fields to obtain boundary conditions for the fine grid region and by an averaging of the tendencies of the prognostic variables on the fine grid to force the coarse grid model. The nested model is applied to two test problems relevant to oceanic phenomena—a barotropic modon and a baroclinic vortex. In each case, nested calculations with 3:1 and 5:1 grid ratios perform quite well, and even ratios of 7:1 are able to reproduce the solution reasonably well while the features are mostly contained within the fine grid region. These results indicate that the interactive nested model approach introduced here may provide an accurate and cost-effective approach to problems that have multiple spatial scales and/or open boundary condition requirements.

1. Introduction

The purpose of this paper is to introduce an interactive, nested primitive equation model for oceanic applications. Models have traditionally been nested in order to increase horizontal resolution in a subregion of the model domain without incurring the computational expense of high resolution over the entire model domain. Nested models fall into two categories, passive and interactive. Passive models use boundary conditions for the high resolution region that have been obtained from a previous low resolution calculation. This class of models is called passive because the coarse resolution flow field affects the fine resolution region by providing boundary conditions for the fine grid domain, but there is no mechanism by which the evolution in the fine resolution region can affect the flow field in the coarse grid (and hence its own boundary conditions). Interactive models, in addition to providing boundary conditions for the fine grid region, allow the evolution within the fine grid to influence the evolution on the coarse grid. Although there are obvious advantages to the interacting systems, they are necessarily more complicated and computationally more expensive.

A single expandable grid is an alternative to nested models and has both advantages and disadvantages relative to the two model approach. An advantage is that the conservation properties of single grid systems are more easily implemented. An advantage of the two model approach is that the fine domain solution depends only on its boundary conditions, which may be carefully examined and documented, and its resolution is everywhere "fine." This may improve (or at least isolate more effectively) reflection properties at the edge of the fine domain compared to a single expanding grid. A potential advantage of the nested two model approach is that there is no constraint to use the same model physics in each region. (Although this option is not used here, there may be certain computational and interpretive advantages to this approach and construction of such a model in the future will require knowledge gained from studies such as the present one.)

Although nested models have a wide variety of potential applications, they may be generalized into two categories. The first type uses the coarse grid to represent a flow field on large space and time scales which influences the evolution within the fine grid region through the boundary conditions. Higher resolution may be desirable in a subregion of the flow field to study small scale phenomena such as mesoscale eddies, instability processes, or interactions with local topography. These models may be either passive or interactive. Meterological nested models have traditionally fallen into this category. The second application uses the fine grid region to model some local process and the coarse grid region primarily provides boundary conditions to allow for flow features generated within the fine grid to propagate outward into the coarse grid. These models must necessarily be interactive since features in the fine grid region must be present in the coarse domain solution for the proper determination of fine grid boundary conditions. In this sense, the nested model provides an alternative approach to the

* NCAR is sponsored by the National Science Foundation.

Corresponding author address: Dr. William Holland, NCAR, Climate and Global Dynamics Division, Oceanography Section, P.O. Box 3000, Boulder, CO 80307-3000.

open boundary condition problem. Both classes are of interest and the methods presented in this paper are potentially of use in both types of applications.

In the past, treatment of the open boundary condition problem for the primitive equations has generally followed two approaches. In one method the region near the boundaries is treated as a highly viscous or sponge layer (Carton 1984; Yoon and Philander 1982). In this way, waves coming into the boundary region are strongly damped and the reflection or generation of spurious waves due to the presence of the boundary is reduced. A drawback of this technique in the present context is that it is very difficult to accurately parameterize the interaction with the surrounding fluid when information is being advected into the region. The second method uses a local phase speed to determine if the variables should be specified as an inflow condition or determined from the interior values as an outflow condition (Orlanski 1976; Engquist and Majda 1979). These inflow/outflow techniques generally involve the use of some type of an advection equation on outflow to determine the value of the prognostic variables on the boundary. Problems arise with this approach when there is no information available about incoming flow fields and when the calculated phase speed approaches zero near the boundary.

A summary of interactive models used in meteorology is given by Zhang et al. (1986). Holland and Vallis (1990) have examined an interactive ocean model using quasi-geostrophic dynamics in the California Current region. Interactive models in which the fine grid region moves to follow a particular feature of interest have been used in meteorology for many years (Ley and Elsberry 1976; Kurihara et al. 1979; Falkovich 1986). Passive nested models have been used in both meteorology (Ross and Orlanski 1982) and oceanography (Spall and Robinson 1989). As these previous studies demonstrate, there are many considerations to take into account in the design of a nested model, including model physics, grid interaction, conservation properties, computational expense, and model applications. We have attempted to justify the choices we have made in our model design but recognize that there are alternatives that we have not explored. A continuing evolution of such models is likely.

This paper is organized as follows: in section 2, the governing equations and solution procedure for the basic model are introduced; the embedding technique is presented in section 3; the embedded model is applied to two example problems of interest in section 4; and the results are discussed and conclusions presented in section 5.

2. The dynamical equations

The embedded models described in this paper use primitive equation physics in both the fine and coarse grid regions. It is assumed that the fluid is hydrostatic and that the Boussinesq approximation is valid. Application of the conservation of momentum to a fluid element is used to derive the x, y, and z momentum equations:

$$\frac{\partial u}{\partial t} + u\frac{\partial u}{\partial x} + v\frac{\partial u}{\partial y} + w\frac{\partial u}{\partial z} + \frac{1}{\rho_0}\frac{\partial p}{\partial x} - 2\Omega v \sin\phi = F_m(u) \quad (1)$$

$$\frac{\partial v}{\partial t} + u\frac{\partial v}{\partial x} + v\frac{\partial v}{\partial y} + w\frac{\partial v}{\partial z} + \frac{1}{\rho_0}\frac{\partial p}{\partial y} + 2\Omega u \sin\phi = F_m(v) \quad (2)$$

$$\frac{\partial p}{\partial z} - g\rho = 0 \quad (3)$$

where u, v, and w are the velocities in the zonal, meridional, and vertical directions, respectively; Ω is the rotation rate of the earth, and ϕ is the latitude. F_m is an as yet undefined parameterization of the viscous forces in the fluid, p is the pressure, ρ is the density, and g is the gravitational acceleration.

Application of the conservation of mass for an incompressible fluid in an Eulerian system of reference with no sources or sinks gives the continuity equation

$$\nabla \cdot \mathbf{u} = 0. \quad (4)$$

The conservation of heat may be written for a fluid without internal heat sources or sinks as

$$\frac{\partial T}{\partial t} + u\frac{\partial T}{\partial x} + v\frac{\partial T}{\partial y} + w\frac{\partial T}{\partial z} = F_h(T). \quad (5)$$

An equation of state is used to calculate density from temperature. The present study has been simplified by not including the effects of salinity, so that

$$\rho = \rho(T). \quad (6)$$

The solution procedure

The procedure used to solve the momentum equations is outlined in this study because it plays an important role in the proper interaction between the model grids. This method was first introduced by Bryan and Cox (1967) and has not been modified in this study. Both the fine and coarse grid models are essentially the GFDL model. For computational efficiency, the surface pressure is eliminated from the equations by decomposing the horizontal velocity field into an internal mode, $\hat{\mathbf{u}}$, and an external mode, $\bar{\mathbf{u}}$,

$$\mathbf{u} = \hat{\mathbf{u}} + \bar{\mathbf{u}} \quad (7)$$

where, for any variable μ,

$$\bar{\mu} = H^{-1}\int_{-H}^{0} \mu dz. \quad (8)$$

Here H is the local depth of the ocean. With this representation, the external mode contains all of the ver-

tically averaged horizontal transport, and the internal mode contains all of the baroclinic structure. The internal mode momentum equations then become

$$\hat{u}_t = u_t - \bar{u}_t \tag{9}$$

$$\hat{v}_t = v_t - \bar{v}_t. \tag{10}$$

The viscous and heat diffusion terms are divided into a horizontal component (F_{mh}) and a vertical component (F_{mz}). The horizontal subgridscale processes are parameterized by a Laplacian friction acting on the velocity components and a Laplacian diffusion acting on the temperature field. The vertical diffusion terms can be written as

$$F_{mz}(\mu_m) = A_{mz}\mu_{zz} \tag{11}$$

$$F_{hz}(\mu_h) = A_{hz}\mu_{zz} \tag{12}$$

where μ_m is internal mode velocity, μ_h is the temperature, and A_{mz}, A_{hz} are diffusion coefficients for momentum and heat.

It is useful to define a volume transport streamfunction Ψ by the following relations:

$$\bar{u} = -\frac{1}{H}\frac{\partial \Psi}{\partial y} \tag{13}$$

$$\bar{v} = \frac{1}{H}\frac{\partial \Psi}{\partial x}. \tag{14}$$

Equations (1) and (2) are integrated in the vertical and cross-differentiated to obtain a prognostic equation for Ψ_t

$$\frac{\partial}{\partial x}\left(\frac{1}{H}\frac{\partial \Psi_t}{\partial x}\right) + \frac{\partial}{\partial y}\left(\frac{1}{H}\frac{\partial \Psi_t}{\partial y}\right) = \frac{\partial \bar{v}_t}{\partial x} - \frac{\partial \bar{u}_t}{\partial y}. \tag{15}$$

The variables are discretized in the horizontal using a B-grid, following the nomenclature of Arakawa and Lamb (1977). In this representation, pressure, density, and transport streamfunction are arranged on grid points and the internal mode velocities are offset one-half grid point in each horizontal direction.

3. The nested model

The nested model is actually two separate models run in parallel. Parallel integration is necessary to achieve the interaction when more than one grid is used. The coarse grid model is the primitive equation model described by Bryan (1969), while the fine grid model is the regional version of that model developed by Spall and Robinson (1989) that introduces open boundaries.

a. Model grids

A schematic of the embedded grids is shown in Fig. 1 for a grid ratio of 3:1. Temperature points are indicated by a plus sign, and internal mode velocity points are indicated by a dot. Each temperature and velocity coarse grid point will coincide with a fine grid point of like type. With an odd grid ratio, the interfaces between adjacent coarse grid points will always coincide with the interfaces of adjacent fine grid points. Although the embedding approach is not limited by this restriction, using only odd grid ratios simplifies the interpolation and interaction between grids. The outermost fine grid point is where the open boundary conditions are specified for the fine grid.

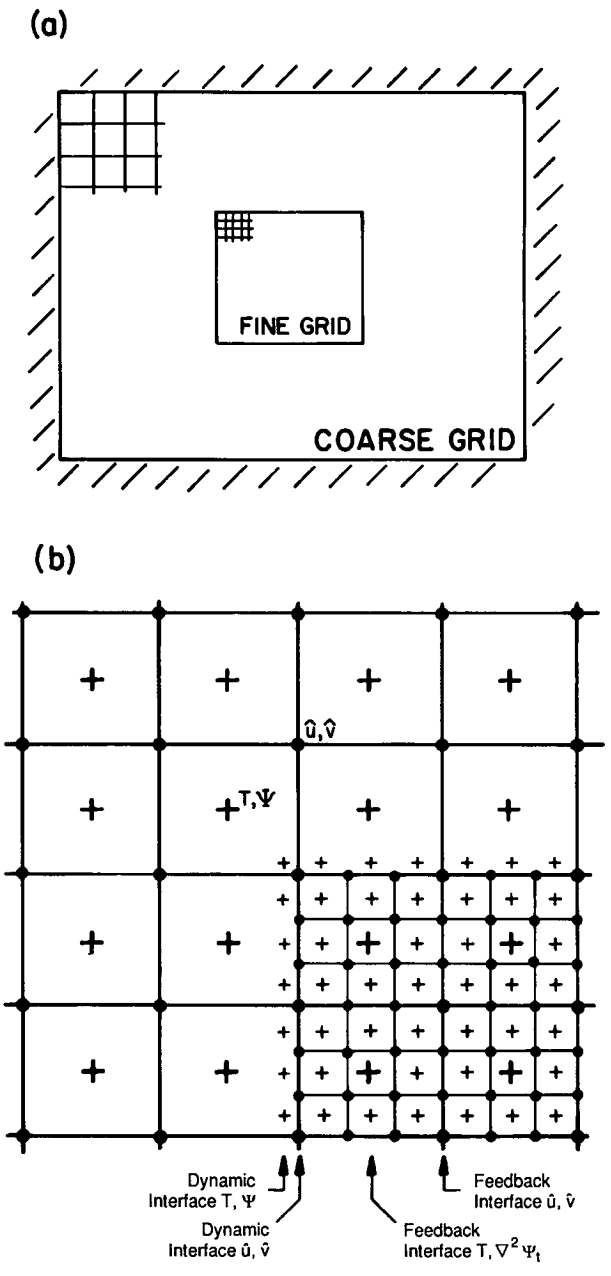

FIG. 1. Schematic of the nested grids: (a) the total domain showing the fine grid model within the coarse grid model; (b) a detail of the overlapping grids for a 3 to 1 ratio of grid sizes.

The feedback interfaces (limit of the region where the fine grid is used to modify the coarse grid) for the internal mode velocity and temperature and barotropic vorticity are separated from their dynamic interfaces (location of the boundary conditions for the fine grid) as shown in Fig. 1b. We have chosen to place the feedback interface as close as possible to the dynamic interface in order to maximize the use of information about the evolution of the fine grid variables in the coarse grid solution. For the baroclinic cases presented here, it was determined that moving the feedback interfaces farther away from the dynamic interfaces results in poorer simulations because information on the fine grid between the dynamic interface and the feedback interface was not transmitted to the coarse grid. This degradation was small for the 3:1 case but increased as the coarse grid size increased because more information was left out of the feedback. The barotropic modon results were not strongly sensitive to this shift of the feedback interface. These results do not disagree with the conclusions of Kurihara et al. (1979) and Zhang et al. (1986) that the feedback interface should be separated from the dynamical interface. However, for the oceanic problems and grid ratios used here, we found that this separation should remain small in order to maximize the information available from the fine grid solution. The grid ratios used in the previous atmospheric studies were relatively modest, 2:1 and 3:1, and would result in only a small neglect of the feedback between grids.

b. Embedding procedure

The embedding procedure is as follows. Because of the implicit nature of the boundary conditions on the transport streamfunction (see Cox 1984), proper interaction between the models requires that the time step for each model be divided into two parts. The first half solves for the internal mode velocity and temperature (baroclinic variables) and calculates the tendency of the barotropic vorticity. The second half uses the vorticity to solve for the barotropic streamfunction. For example, suppose we have information on u, v, Ψ, and T at time step n on both grids. First we compute the baroclinic variables $\hat{u}^{n+1}$, $\hat{v}^{n+1}$, and T^{n+1} in the fine and coarse regions. The fine grid boundary conditions are explicit and have been obtained from the coarse grid variables at time step n. The newly calculated tendencies of the baroclinic variables and barotropic vorticity on the coarse grid are replaced with the spatial average of the corresponding fine grid quantities. For example, the tendency of the coarse grid temperature ($\dot{T}_c$) would be determined by the tendencies of the coincident fine grid temperatures ($\dot{T}_f$) over the area of the coarse grid box (A) as

$$\dot{T}_c = \frac{1}{A}\int_A \dot{T}_f dA. \tag{16}$$

For the 3:1 grid ratio, $\dot{T}_c$ would be the average over nine (3×3) fine cells, suitably weighted by their areas.

The coarse grid barotropic streamfunction is now solved over its entire domain using the updated (averaged) tendency of the barotropic vorticity in the region of the fine grid and the original coarse grid tendencies everywhere else. The barotropic streamfunction on the fine grid is then obtained using the fine grid vorticity tendency with boundary conditions interpolated from the new coarse grid streamfunction.

The authors believe this technique best represents the net effect of the fine grid evolution on the scale of the coarse grid. The heating or cooling of a water parcel (with no surface heat flux) is due to the net horizontal and vertical advections and diffusions through the sides of the grid box. By averaging the temperature tendency instead of temperature, the heating of the coarse grid parcel is consistent with the net heat flux through the sides of the coarse grid as represented on the fine grid. The fluxes across each fine grid interface within the coarse grid box cancel out and the net contribution is due to fluxes through the outermost edge of the coarse grid box. In addition, the net flux out of each side of the coarse grid box is equal to the net flux across the side of each neighboring grid box. Similarly, the acceleration of the coarse grid parcel is due to the net momentum flux through the boundaries, the imbalance in the geostrophic terms, and the average of horizontal and vertical diffusion. The contribution due to the imbalance in the geostrophic terms is an average of the acceleration at each fine grid point rather than the acceleration that would occur from the average pressure gradient and Coriolis terms.

Using an interpolation of the coarse grid variables to obtain the open boundary conditions for the fine grid model does not conserve fluxes of mass, heat, or momentum at the interface between the two models. The fluxes through the interface into the fine grid region will not be the same as the flux calculated through the same interface from the coarse grid variables. Boundary conditions can, in principle, be developed for this model that ensure that the net flux through each subset of fine grid boundaries adds up to the flux through the corresponding coarse grid interface. So far these conservative schemes have not produced stable integrations. Only a few atmospheric nested models conserve mass and momentum fluxes by making use of the "box" method first developed by Koss (1971). The box method was adapted for staggered grids by Sobel (1976), but the method becomes quite complex due to handling of the momentum boxes at the interface. As pointed out by Zhang et al. (1986), it may be necessary to sacrifice exact conservation between the two grids in order to obtain a smooth, stable solution. For short time integrations, such as those presented in this study, it is not believed that exact conservation properties are critical. For long time integrations, such as

global and basin scale climate studies, conservation is likely to be a more important issue.

There are several reasons for integrating the models in the above fashion. The entire coarse grid is calculated at each new time step even though the points coincident with the fine grid are subsequently modified. This allows for only minor modifications of the coarse grid model and maintains code properties desirable for vector processing machines. Using only an odd integer number of fine grid points per coarse grid spacing results in a more efficient integration technique for the feedback between the two model B grids. The explicit nature of the baroclinic boundary conditions and the implicit nature of the barotropic boundary conditions are preserved in the fine grid by solving each time step in two parts. In the present version of the model, the coarse grid uses the same time step as the fine grid. Although numerical stability considerations would allow for a larger time step on the coarse grid, we have chosen not to implement this option because, given that the coarse grid contributes little to the overall computational expense, it would add an additional level of complexity for very little gain.

4. Model calculations

In this section the nested model is applied to two test problems. There are many possible applications that are of interest both from an oceanographic and a computational point of view. The examples shown here are not intended to address all of the interesting issues that may arise in the application of nested models; rather, they were motivated by their relative simplicity, knowledge of expected behavior, general relevance to oceanic phenomena, and previous experience with open boundary condition simulations. The first test case is initialized with a barotropic modon (Flierl et al. 1981) within the fine grid region. The modon then propagates to the east through the boundary interface and into the coarse grid region. The second problem is initialized with an anticyclonic baroclinic vortex within the fine grid and allowed to evolve until the vortex has propagated into the coarse grid region. In both cases, a two-level model is used in the vertical direction. The first problem is of the type in which a flow field of interest is contained within the fine grid region and the coarse grid acts primarily as a means to obtain open boundary conditions. The second also starts with information within the fine grid but generates large scale features which propagate into the coarse grid and, in time, feed back and provide large scale forcing for the evolution of the fields within the fine grid region. In each of these experiments, the propagation of the features is strongly dependent on the structure of the features themselves. If the structure breaks down, the solution will quickly diverge from the reference case. In this sense, the results will be very sensitive to errors and thus provide a strong test of the nesting procedure.

a. Barotropic modon

For the first application, the nested model is initialized with a barotropic modon within the fine grid. The model is then run ahead in time until the modon has passed fully out of the fine grid and into the coarse grid. An advantage of this test problem is that an analytic solution to the barotropic modon on a quasi-geostrophic beta plane is known (Flierl et al. 1981). However, the model will not reproduce this exact solution for several reasons. The model grid is not infinite in horizontal extent, the model contains full primitive equation physics, the continuous solution is represented by a finite number of grid points, and horizontal dissipation is present (required for numerical stability). Nevertheless, these differences are expected and found to be small so that the analytic solution provides a good benchmark for the model calculations.

The beta-plane analytic expression for the streamfunction of a barotropic modon situated at the origin at time zero is written in polar coordinates (r, θ) as (Flierl et al. 1981)

$$\psi = H_0 C \sin(\theta)\left[\frac{a\beta J_1(kr)}{k^2 C J_1(ka)} - \left(1 + \frac{\beta}{k^2 C}\right) r\right], \quad 0 \leq r \leq a \tag{17}$$

$$\psi = H_0 C a \sin(\theta)\left[-\frac{K_1\left(r \Big/ \left(\frac{C}{\beta}\right)^{1/2}\right)}{K_1\left(a \Big/ \left(\frac{C}{\beta}\right)^{1/2}\right)}\right], \quad r > a. \tag{18}$$

This modon will propagate eastward at a uniform speed C. The parameters that we used to define the modon are

$$a = 1.0 \times 10^7 \text{ cm}, \quad \beta = \frac{2\Omega}{a_r}\cos(\theta_m),$$

$$\theta_m = 38.5°\text{N}, \quad H_0 = 5 \times 10^5 \text{ cm},$$

where Ω is the rotation rate of the earth and a_r is the radius of the earth. This give a constant eastward translation for the modon of $C = \beta a^2 = 17.85$ cm s^{-1}.

Three experiments are carried out with grid ratios of 3:1, 5:1 and 7:1 between the fine and coarse resolutions, referred to as M3, M5 and M7, respectively. The model parameters are summarized in Table 1 for each calculation. The coarse grid domain is approximately 1540×1540 km^2 and the fine grid domain is approximately 620×620 km^2, centered on the initial modon position. The domain sizes with different ratios between fine and coarse resolution are not exactly the same due to changes in the coarse grid spacing and constraints on interfacing the fine and coarse grids. The initial position of the modon and the location of the fine grid region in the coarse grid domain are shown in Fig. 2. The grid spacing in the fine grid of 5 km

TABLE 1. Fine and coarse model parameters for modon experiments, diffusion coefficients units $cm^2\ s^{-1}$.

	Fine				Coarse			
Run	M, N	$\Delta_x\Delta_y$ (km)	A_h	A_z	M, N	$\Delta_x\Delta_y$ (km)	A_h	A_z
M3	125	5	1×10^5	0	103	15	2.5×10^5	0
M5	127	5	1×10^5	0	63	25	1.0×10^6	0
M7	121	5	1×10^5	0	45	35	2.0×10^6	0

resolves the modon quite well with 40 grid points across its diameter. The coarse grid spacings increase from 15 km to 25 km to 35 km in the three experiments. The first case gives approximately 13 grid points across the modon, the second 8, and the third less than 6. McWilliams et al. (1981) found that 15 grid points per modon diameter were required to reproduce the phase speed to within 10% of its analytic value in a doubly periodic beta-plane quasi-geostrophic model. Based on their results, the first coarse grid should represent the modon fairly well, the second marginally, and the third rather poorly. The horizontal diffusion coefficients have been increased in the coarse grids to maintain numerical stability.

The transport streamfunctions for the analytic solution and for the fine grid region of experiment M3 are shown in Figs. 3a and 3b for days 10, 20 and 30. The structure of the modon is maintained quite well in the model calculation. The main difference is that the propagation speed is approximately 3% faster in the model solution than it is for the analytic solution. There is no visible distortion of the modon as it encounters the boundary between the fine and coarse grid regions, and it leaves behind little evidence of its passage after it has left the fine grid region. The second and third experiments (M5 and M7) show similar behavior in the fine grid region although there are some noticeable distortions of the modon as it passes through the grid interface (Fig. 3c and 3d). While the modon is contained within the fine grid, calculations M5 and M7 reproduce the modon structure quite well. As the modons pass through the boundary, their phase speed decreases slightly and they become distorted. The modon passes completely through the boundary in M5 but not quite all the way through in M7.

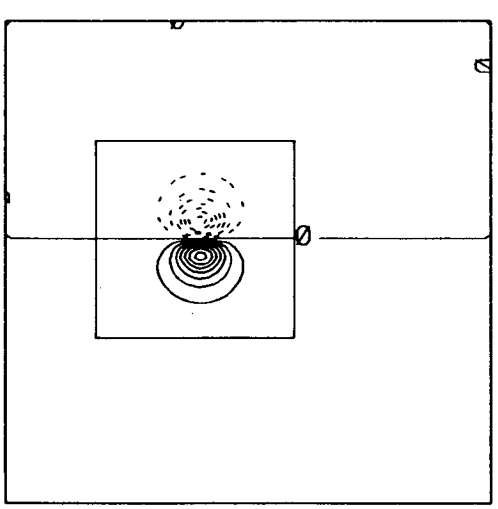

FIG. 2. Modon initial condition in the coarse grid; the fine grid domain is indicated.

The root-mean-square (rms) percentage error (normalized by the rms of the initial streamfunction field) over the fine grid region for each of the experiments is shown in Fig. 4. Over the first 10 days the error increases almost linearly in each case due to the difference in phase speeds between the model results and the analytic value. On day 10 the modon is beginning to interact strongly with the interface and enter into the coarse grid. The errors in M3 level off at about 10% while M5 increases to 15% and M7 increases to over 20% on day 20. After the peak of the modon has passed through the interface, the rms error begins to decrease since the whole solution is decreasing in the fine grid. The highest resolution experiment (M3) levels off after day 25 at about 2%. The second case (M5) decreases to 5% but then begins to increase slightly again at the end of the experiment. The third case (M7) decreases until day 25 but then rapidly increases to almost 40% by day 30. It is believed that this increase is due to contamination of the fine grid solution by westward propagating Rossby waves that were generated in the coarse grid after the modon broke down (see next paragraph). The error again decreases as dissipation begins to act on these features and they broaden in scale.

The coarse grid representation for each of the nested calculations is shown in Figs. 5b, 5c, and 5d along with the analytic solution (Fig. 5a) again for days 10, 20, and 30. For plotting purposes, only part of the coarse grid region is shown—that part which contains the modon. The northern, southern, and western boundaries in the figure are coincident with the extent of the fine grid model, while the location of the eastern interface with the fine grid is the middle line indicated on the figure. On day 10 the modons are still within the fine grid region, and they are represented well in each of the experiments. On day 20, the modons have almost left the fine grid and mostly exist in the coarse grid region. Experiment M3 still compares well with the analytic solution while M5 shows some decrease in amplitude and M7 has weakened considerably and

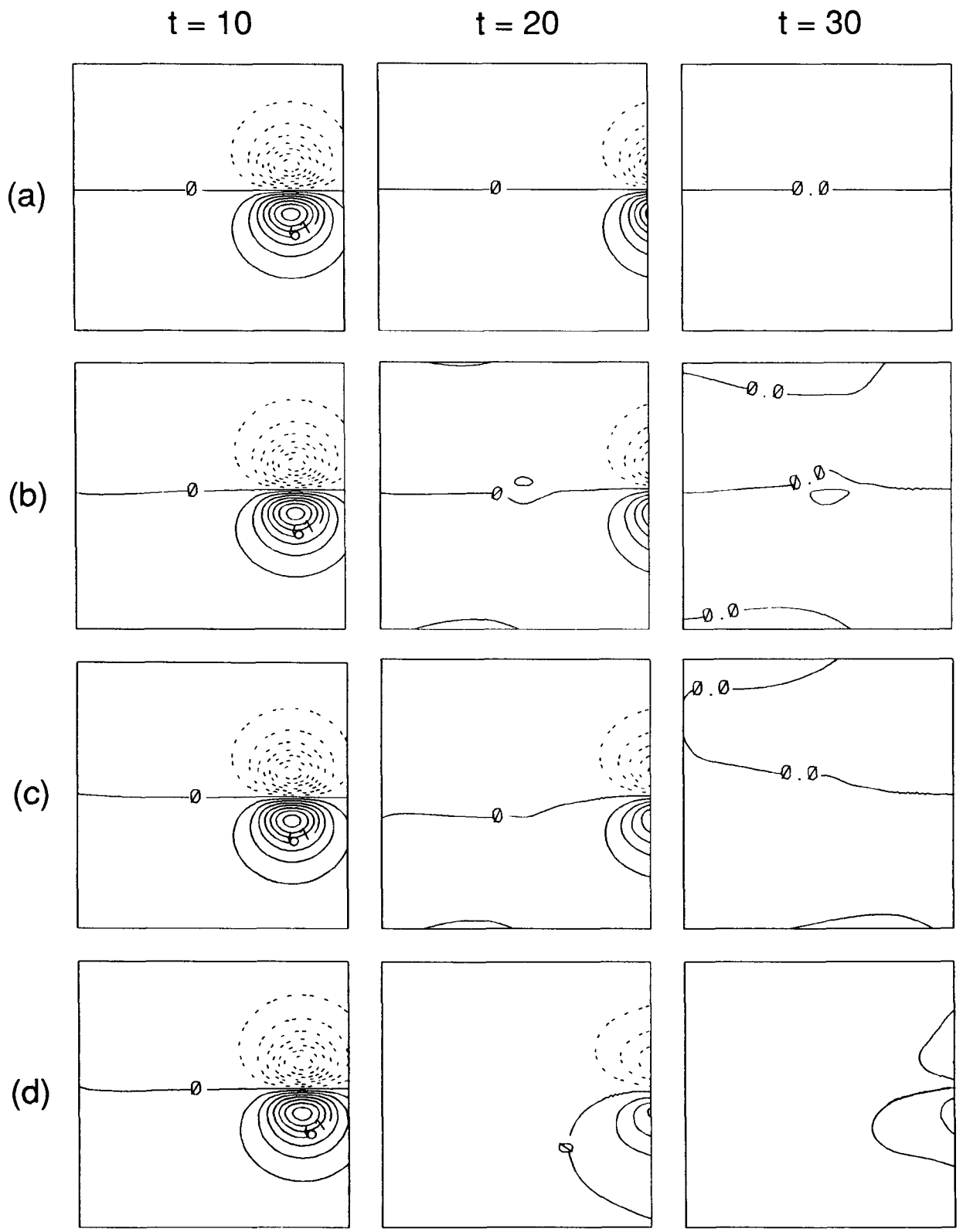

FIG. 3. Transport streamfunction in the fine grid region on days 10, 20, and 30: (a) analytic solution, (b) M3, (c) M5, (d) M7.

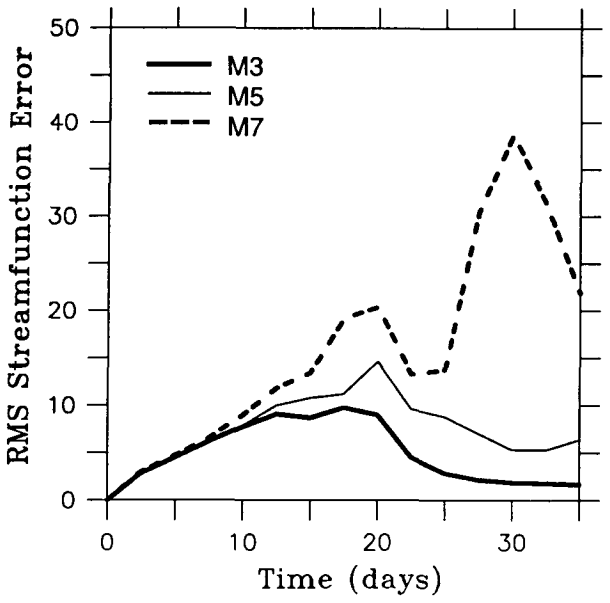

FIG. 4. Rms streamfunction difference for the modon calculations in the fine grid.

becomes seriously distorted. The modon has passed fully into the coarse grid by day 30. As one would expect, M3 is still representing the modon well, M5 is losing amplitude and beginning to enlarge, and M7 has broken down into complex, multiple circulations. Since the flow field in M7 no longer even begins to satisfy the modon relation, these features begin to disperse as westward propagating Rossby waves. This behavior in the coarse grid is consistent with previous numerical experiments with modons carried out by McWilliams et al. (1981). Because of the interaction between the grids, these features enter the fine grid region near the end of the experiment. These results demonstrate that the feedback from the fine grid to the coarse grid maintains the modon structure even when the coarse grid does not have sufficient resolution to do so on its own. This feedback is necessary in order for the coarse grid to provide good boundary conditions to the fine grid.

b. Baroclinic vortex

There is no analytic solution available for the evolution of a baroclinic vortex. As a result, the performance of the nested model calculations will be evaluated against a single grid, high resolution model calculation that we call our "reference solution." The nested calculations use grid ratios of 1:1, 3:1, 5:1 and 7:1, called V1, V3, V5 and V7, respectively. The coarse grid domain is 1800 km by 1800 km while the fine grid region is approximately 580 km by 580 km. The numerical parameters are summarized in Table 2. Note that the reference solution and case V1 are not identical calculations. Experiment V1 is used to determine what differences are introduced to the calculation due only to the nesting technique with no changes in grid resolution by comparison with the single grid calculation using the same resolution. It turns out that this difference is small and errors in the subsequent calculations are, in essence, entirely a result of the difference in grid sizes.

The initial vortex is described by a Gaussian pressure distribution with maximum geostrophic velocity of 100 cm s^{-1} and a horizontal e-folding scale of 60 km in the upper layer and no motion in the lower layer. The velocity field is initialized to be in geostrophic balance with the Gaussian pressure distribution. Temperature is derived from pressure through the hydrostatic equation and the equation of state, Eqs. (3) and (6).

The evolution of the ring in the reference calculation is shown in Figs. 6a (streamfunction) and 6b (temperature). The whole domain is shown. Because the streamfunction is more variable in time, it is shown at 20-day intervals while the temperature is shown only on days 0, 60, and 100. The location of the fine grid domain to be used in the subsequent nested experiments is indicated in both the streamfunction and temperature plots. Early in the experiment the temperature field shows only slight adjustments while the transport streamfunction begins to develop a radiating barotropic wave pattern. The ring moves steadily to the southwest as the barotropic wake continues to develop and extend toward the boundaries. On day 40 the wake begins to interact with the solid walls of the larger, coarse domain and reflects back into the interior. By day 60 the barotropic circulation is quite complicated as a result of the reflected waves interacting with the wake pattern. Meanwhile, the baroclinic ring has moved to the southwest and its maximum temperature has slowly decreased due to horizontal diffusion. The streamfunction field (barotropic flow) continues to disperse until, by day 100, no ring feature is recogniz-

TABLE 2. Fine and coarse model parameters for vortex experiments; diffusion coefficients units $cm^2\ s^{-1}$.

	Fine				Coarse			
Run	M, N	$\Delta_x\Delta_y$ (km)	A_h	A_z	M, N	$\Delta_x\Delta_y$ (km)	A_h	A_z
V1	59	10	5×10^5	5	181	10	5×10^5	5
V3	59	10	5×10^5	5	61	30	5×10^6	5
V5	62	10	5×10^5	5	37	50	12.5×10^6	5
V7	58	10	5×10^5	5	26	70	25×10^6	5

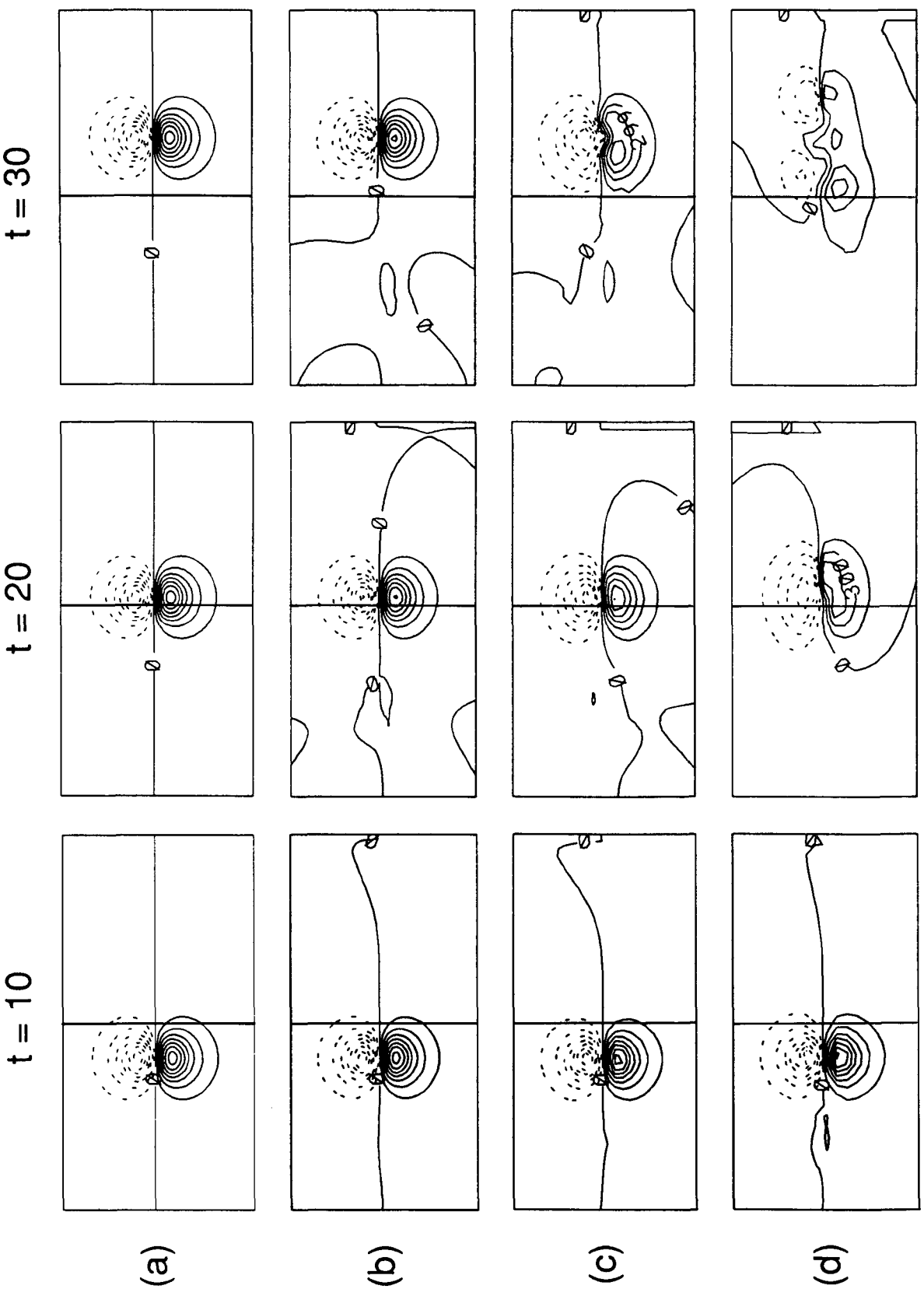

FIG. 5. Streamfunction in the coarse grid domain on days 10, 20, and 30: (a) analytic solution, (b) M3, (c) M5, (d) M7. The north and south boundaries shown here are not the actual domain boundaries (see Fig. 2).

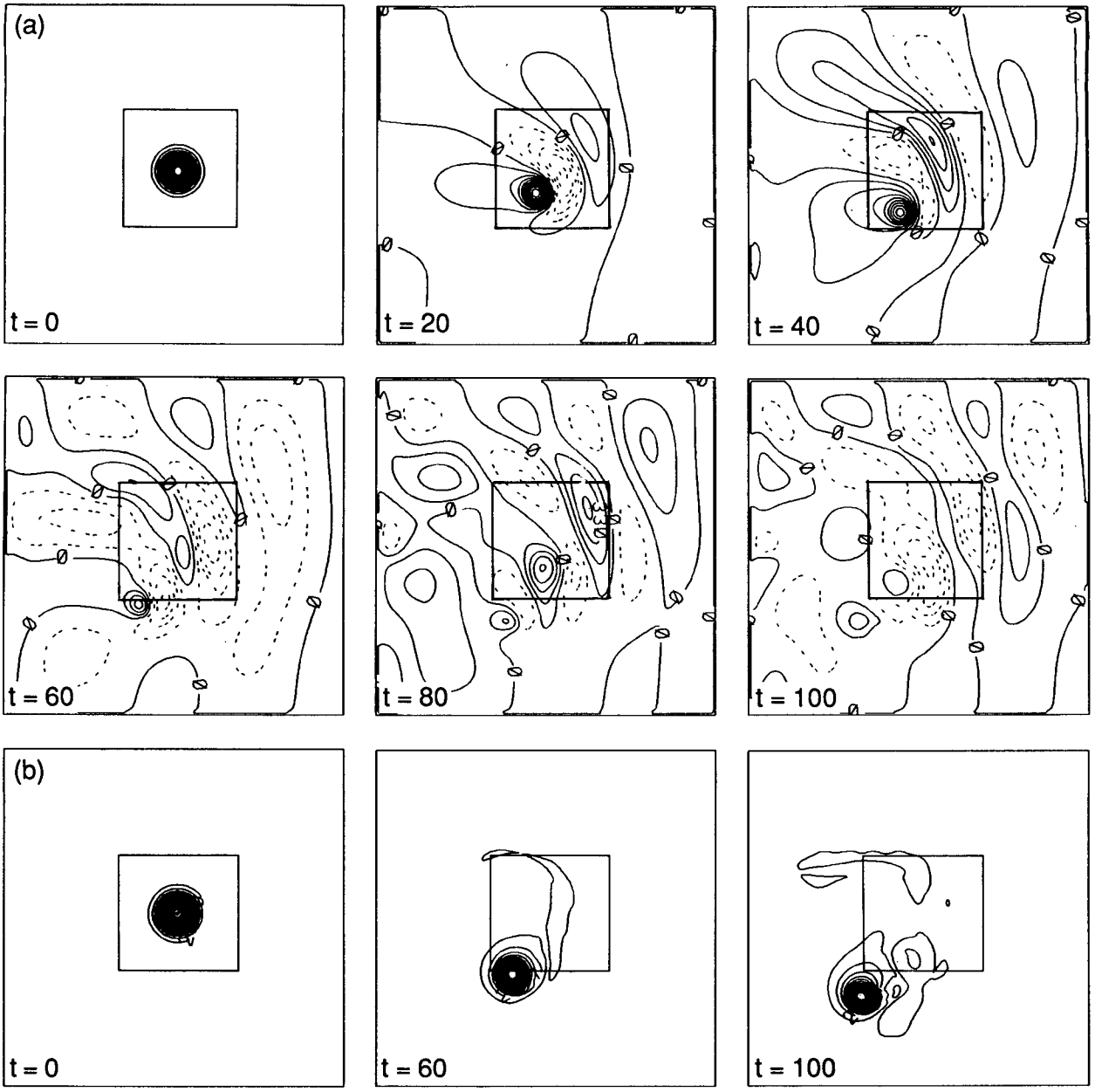

FIG. 6. Reference calculation for the baroclinic vortex: (a) transport streamfunction at days 0, 20, 40, 60, 80, and 100; (b) temperature at days 0, 60, and 100. The small interior box shows the fine domain that will be used in subsequent experiments.

able out of the background eddy field. The temperature field (baroclinic flow) maintains its integrity as it moves southwest.

The fine grid region of V3 and the difference between the nested calculation and the reference calculation are shown in Fig. 7 at 30-day intervals. The baroclinic ring begins to interact with the boundary on day 30 and until this time the nested calculation is essentially the same as the reference calculation. The difference fields remain at less than one contour level (8% of the maximum ring temperature) until day 40 (not shown). Eventually the temperature of the ring becomes too cold and, by day 60, this difference is clearly related to the inflow portion of the interface. In addition, some small scale errors are found near the outflow part of the ring. This behavior may be due to an overspecification of the boundary conditions at outflow points and the inability of the coarse grid to supply properly matched values. Another 3:1 experiment was carried out using open boundary conditions that advect vorticity on outflow (Spall and Robinson 1989) but these small scale errors were found in that calculation also.

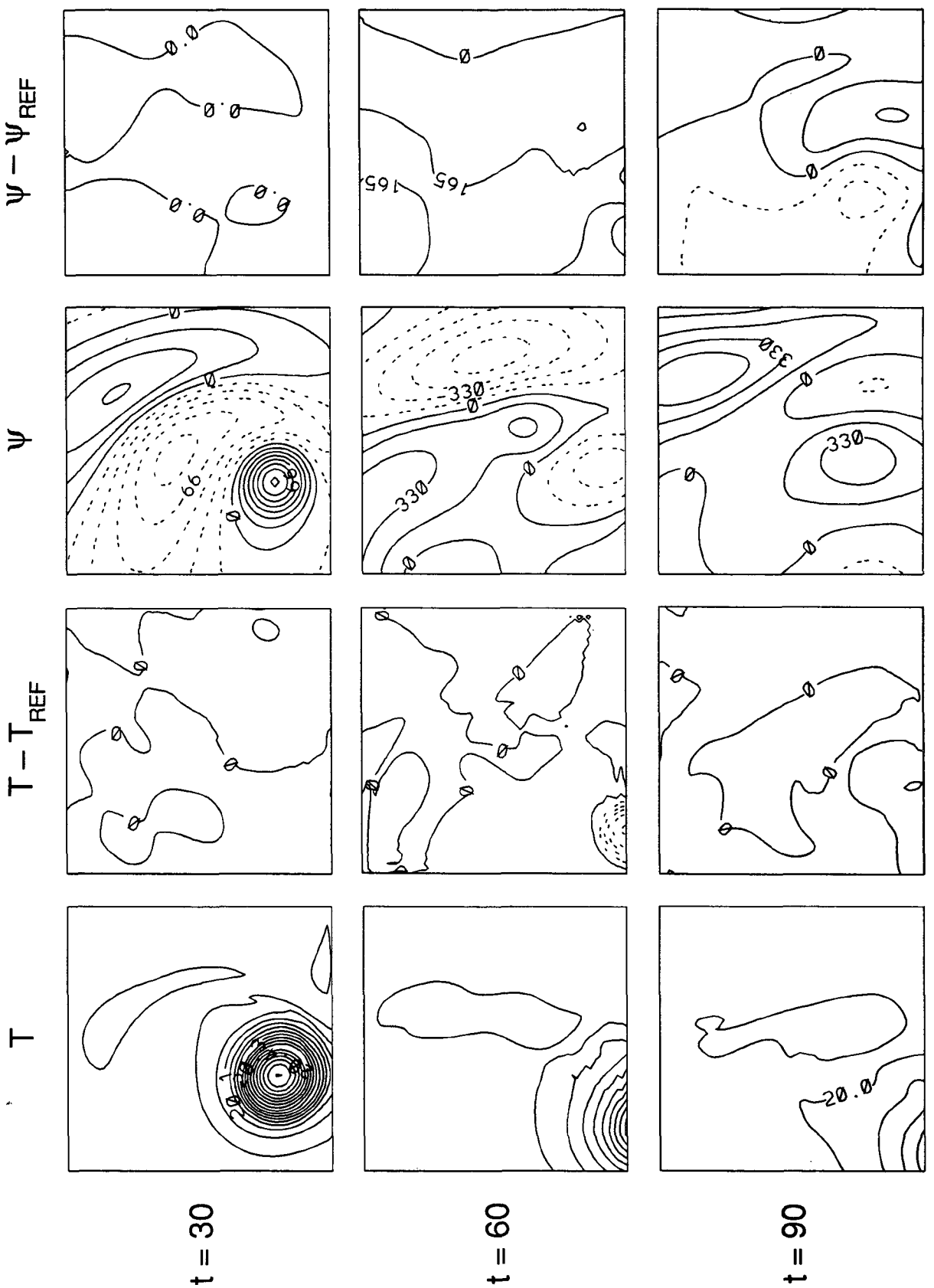

FIG. 7. The V3 temperature and streamfunction fields and their differences from the reference calculation for the fine grid region. The contour interval in the temperature maps is 0.04°C and in the streamfunction maps 16.5×10^{12} cm^3 s^{-1}. The same contour interval is used in the fields and the differences.

This difference field is characteristic of the central portion of the experiment, days 40–60. The temperature perturbations are confined largely to the inflow region of the boundary while the transport streamfunction differences exist on both this intermediate scale and also on a much larger scale. The large scale streamfunction errors are probably due to the somewhat poor representation of the Rossby waves in the coarse grid and not directly related to the interface boundary condition. For the remainder of the experiment, the temperature errors become positive and exist on the same scale as the ring. This occurs because the ring propagates too slowly once it is most of the way into the coarse grid. This is also seen in single grid calculations at the coarse resolution and is not directly related to the nesting technique. The streamfunction errors remain on quite large scales and, again, are probably due to the somewhat poor representation of the wake in the coarse grid.

Temperature and streamfunction maps for calculations V5 and V7 are not shown because they qualitatively follow those of V3. Instead, we will evaluate the performance of the nested models in the fine grid region by following the location and value of the maximum temperature of the ring. The maximum temperature of the ring for the reference calculation and each of the nested experiments is shown in Fig. 8a. After the initial adjustment period, the maximum temperature in the reference calculation very slowly decays until almost day 60. At this time the center of the ring is passing through the grid interface and the maximum temperature found anywhere in the fine grid region rapidly decreases due to the fact that the eddy leaves the region. The nested experiments V3 and V5 follow the reference calculation quite well until day 42, when the temperature begins to decrease earlier than, but not as quickly as, that in the reference calculation. The temperature decrease begins earlier because the portion of the ring that has moved into the coarse grid is feeding back onto the fine grid solution. The temperature continues to decrease as the ring passes through the interface into the coarse grid region. The temperature does not decrease as much at the end of these experiments as it did in the reference solution because the ring, once in the coarse grid, moves to the southwest more slowly and remains closer to the fine grid region. Experiment V7 feels the interaction with the coarse grid sooner, on day 35, but eventually passes through the boundary at about the same time. Experiment V3 is the warmest at the end of the calculation, even though its center is the furthest away from the fine grid, because the horizontal diffusion in the coarse grid has not decreased the ring amplitude in this experiment as much as it did in the other nested calculations (see Fig. 10).

The location of the maximum temperature of the ring in the fine grid (we will call it the ring center) is shown in Fig. 8b for the reference and each of the nested

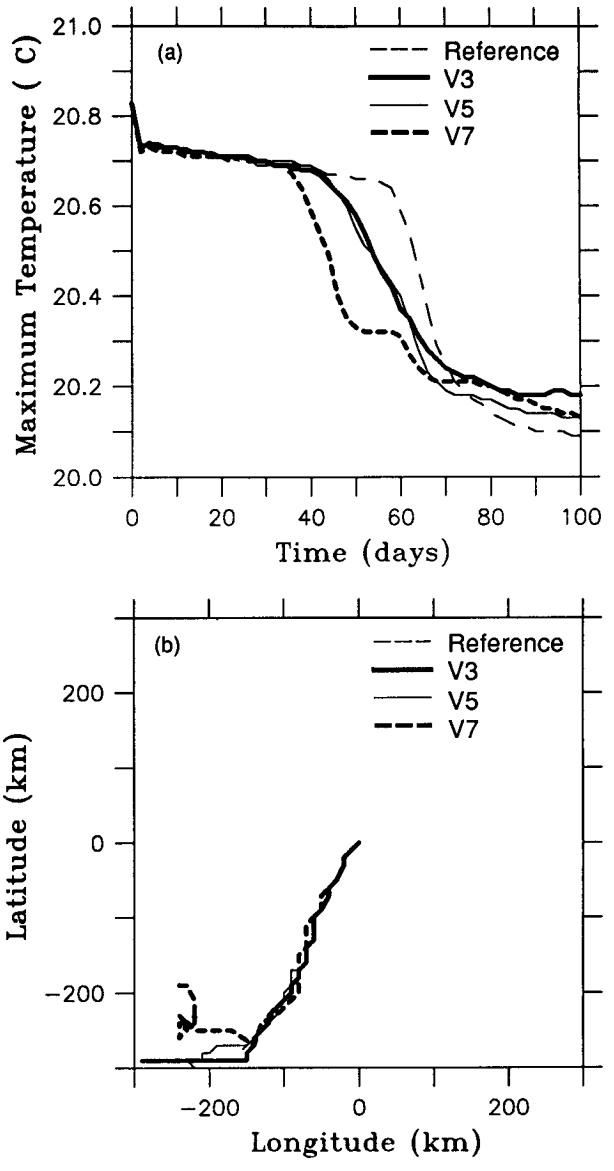

FIG. 8. Value (a) and location (b) of the maximum temperature for the fine grid vortex experiments.

experiments. The rings are tracked until they pass through the interface (at 300 km distance). Experiment V3 follows the track of the reference calculation almost exactly throughout the entire simulation (in fact, the path of the reference calculation is obscured by the path of V3 in our diagram), while V5 remains within 20 km of the reference track. In Experiment V7, the vortex does not move far enough to the west when it is approximately 100 km away from the southern interface and then appears to have trouble passing through the southern interface (moves westward only) for the remainder of the experiment.

The percentage rms errors over the fine grid region for the temperature are shown for each of the experi-

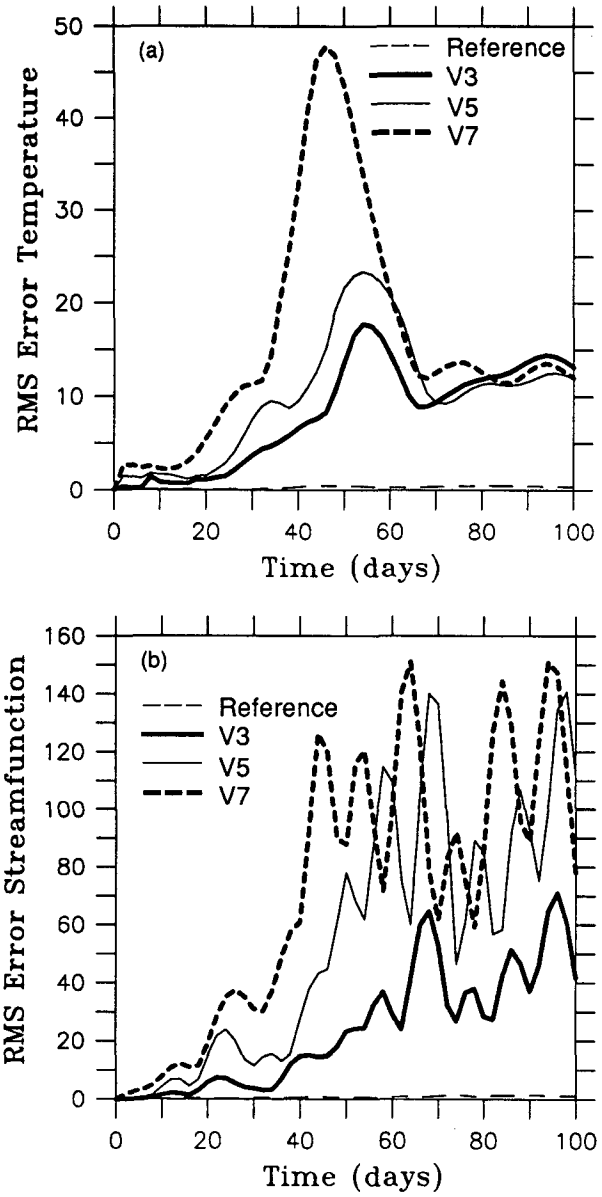

FIG. 9. Rms difference for the vortex calculations in the fine grid: (a) temperature; (b) transport streamfunction.

ments in Fig. 9a. The errors have been normalized by the rms of the initial temperature field minus the background temperature. Calculation V1 (the case with two models but a single grid size, here marked Reference) maintains an error of less than 1% for the duration of the experiment, compared to the reference case. Each of the other experiments show similar patterns to each other, with the errors increasing faster in the coarser grid resolutions. An initial growth period occurs over the first 2 days, caused by the adjustment of the ring initial condition to the discrete grid. Between days 2 and 15 the errors remain small and almost constant. This is the period during which the baroclinic ring is propagating to the southwest and is contained mostly within the fine grid region. At day 15 the ring begins to feel the grid interface and the errors begin to grow, most rapidly for V7, followed by V5 and V3. The errors increase to a maximum near the time the center of the ring is passing through the interface. The maximum error for V3 is 18% while V5 and V7 increase to 23% and 47%, respectively. After the center of the ring has passed through the interface, the errors decrease rapidly, simply reflecting the fact that the rings continue to leave the fine grid region even after they are mostly contained in the coarse grid.

The percentage rms errors (normalized by the rms of the streamfunction in the initial conditions) over the fine grid for the transport streamfunction are shown in Fig. 9b. For run V1 (here marked Reference), the error remains at approximately 1% throughout the experiment. The other three calculations exhibit a smooth initial growth period over the first half of the experiment and then highly variable errors over the second half. During the smooth growth period, each of the calculations shows a sharp increase between days 15 and 25. This is the period when the rapidly developing barotropic wake is extending into the coarse grid region. After this increase, the errors decrease slightly before jumping up very sharply at day 40 (V5 and V7) and day 60 (V3). This is roughly coincident with the time at which the barotropic ring passes through the interface. For the remainder of time the errors are highly variable, as a result of waves reflecting off the solid boundaries in the coarse domain and propagating back into the fine grid region. Although these reflections are also present in the reference calculation, the ability of the model to accurately resolve the structure and phase speed of these waves is dependent on the horizontal resolution in the coarse grid region. The accurate reproduction of these wave reflections will become less important for increasingly larger coarse grid domains (basin scale simulations) in which distant dissipation precludes reflected waves returning to the fine region.

In the coarse grids, the initial structure of the ring is not as well represented as it was in the fine resolution grid. However, the early development of the ring and its associated circulations are quite similar to the reference case in both the temperature and streamfunction fields. This is because it is maintained by feedback from the fine domain. There is little noticeable distortion of the baroclinic vortex as it encounters the grid interface but the strength of the ring is quickly reduced as it continues into the coarse grid in each experiment (not shown). Because the main focus of this study is the ability of the model to reproduce the fields in the fine grid region, a detailed examination of the coarse grid representation will not be made. It is of interest, however, to determine how well the ring is represented in the coarse grid while it is coincident with the fine grid region. The ability of the fine-to-coarse grid feedback to maintain the proper ring structure in the coarse grid

is necessary in order for the interactive system to provide adequate boundary information for the fine grid calculation.

The coarse grid evolution of the vortex is summarized for each of the experiments by monitoring the value of the maximum temperature of the ring (Fig. 10) as a function of time for each of the experiments. The reference run shows a sharp decrease over the first 2 days and then a gradual reduction as dissipation and heat diffusion decrease the temperature of the ring. Each of the nested experiments shows an initial adjustment, a period of gradual decay, and finally a more rapid decrease for the remainder of the experiment. The initial adjustment in the nested calculations results in a lower temperature because the peak is not as well represented by the coarser grids. The gradual decay occurs while the ring is contained within the fine grid region and the nested interaction is controlling the ring evolution in the coarse grid. As the ring begins to cross the fine–coarse grid interface, the amplitude of the ring decreases due to a combination of coarser grid resolution and increased diffusion. This is reflected by the rapid decrease in maximum temperature beginning on day 42 for experiment V3, day 40 for V5, and day 30 for V7. As the rings move entirely into the coarse grid (after day 50) their amplitudes are greatly reduced as a result of the coarse representation and stronger horizontal diffusion. The location of the maximum temperature of the ring (not shown) is reproduced quite well for each of the experiments while the ring is contained within the fine grid region.

It is also of interest to compare the coarse grid representation in a nested calculation with a single grid calculation that uses the same coarse resolution every-

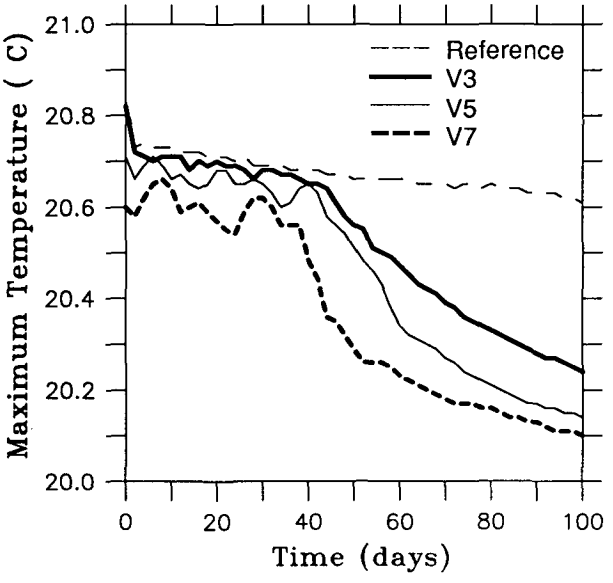

FIG. 10. Maximum temperature for the coarse grid vortex experiments.

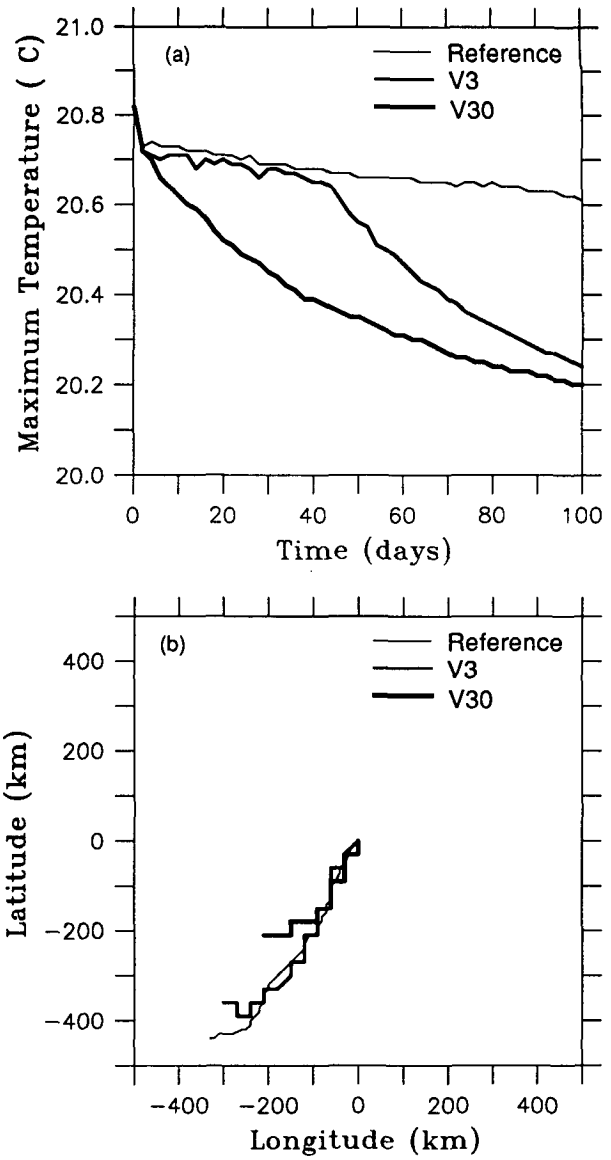

FIG. 11. Value (a) and location (b) of the maximum temperature for the coarse grid vortex experiments.

where. This gives us an indication of the effectiveness of the feedback mechanism and the benefits of the nested model approach. Figure 11a shows the maximum temperature for the reference calculation, the nested calculation V3, and a calculation with 30 km everywhere, V30. The ring amplitude is damped very quickly in V30 while the nested calculation closely follows the reference calculation for the first 40 days (while the ring is within the fine grid). The locations of the ring centers in these three experiments are shown in Fig. 11b. Calculation V3 follows the reference quite well while it is within the fine grid and fairly well for another 150 km after it enters the coarse grid. Run V30 follows the correct path for approximately 150

km but then turns sharply to the west and stalls. It is clear from these figures that the single grid calculation at 30 km resolution performs rather poorly when compared to both the fine and coarse grid solutions in the nested calculation V1.

The issue of how to specify the subgridscale parameterizations in the fine and coarse regions is a difficult one. If possible, it would be desirable to maintain the same physical assumptions between the model grids (i.e., the same diffusion coefficients). However, using a subgridscale parameterization that will yield numerically stable solutions at both fine and coarse grid resolutions will probably result in stronger damping of the fine grid region than would otherwise be needed or wanted. Hence, there must be a tradeoff between these physical and numerical considerations. For the baroclinic vortex experiments discussed in this section, using the fine grid diffusion coefficients in the coarse grid results in the growth of unrealistic small scale errors. However, parameters intermediate to the fine and coarse values used here can be found that will result in stable solutions with less viscous damping in the coarse grid region. No attempt has been made to "tune" the model parameters in order to obtain the least diffusive, computationally stable solution in the coarse grid.

5. Discussion and conclusions

In order to adequately resolve important time and space scales of oceanic circulation, it is often necessary to make use of very high resolution in numerical ocean models. As a consequence, it may be useful and even necessary either to isolate a local domain by inventing somewhat ad hoc boundary conditions that parameterize the influence of the rest of the ocean on the domain of interest (e.g., Robinson and Walstad 1987; Holland 1986) or to develop a numerical construction that has variable resolution (e.g., the GFDL ocean circulation model). In the former case, certain characteristics of the flow must be known at the open boundary to properly handle the developing fields in the interior and the propagation of features across the open boundary, as well as to properly include the influence of the outer ocean on the domain of interest. In the latter case, the changing resolution can pose a problem for the propagation of information across the juncture of the fine and coarse numerical resolutions, although certain information from the outer domain can *force* the inner one, at least for some space and associated time scales.

In this paper, we have taken a somewhat different approach for a primitive equation model. This approach is to run a pair of calculations simultaneously, one for the *large scale* flow (a future example might be the North Atlantic) and another for the *fine scale* flow (say, the Gulf Stream region). The two models are, in fact, separate models but they interact. The fine resolution model occupies part of the physical domain of the coarser resolution model. The two regions interact through a feedback process that allows the fine region to develop its fine resolution phenomena while being forced by the coarse resolution solution only at its boundaries, which are interior to the coarse model. Simultaneously, the fine resolution solution is used to replace, in an averaged sense, the rate of change of the prognostic variables in the region common to the two models, so that the coarse model has similar (if somewhat averaged) features in the common part of the total domain.

The technique appears to work quite well in the cases examined here. The eddy structures and their development in time clearly need the high resolution to behave properly. The presence of the larger scale coarse domain allows the eddy structures to leave the fine resolution region relatively cleanly, at least for resolution differences of 3:1 and 5:1. This has large consequences for the economy of carrying out these calculations. At a 3:1 resolution difference, the coarse resolution part of the calculation is effectively one-ninth the cost in computer resources per unit area covered (given that the time step is kept equal in the two calculations). Thus the larger domain could be many times larger than the fine one, or alternatively, the net cost of the coarse part of the calculation could be a small fraction of the total computational cost. Effectively, this could be considered a way to provide nearly correct boundary conditions to the fine resolution model.

Two test problems were examined. The first was a barotropic modon (Flierl et al. 1981) initialized in the fine domain and allowed to propagate out. The advantage of the modon is that there is an analytic solution to test against so that the net effect of all numerical errors (even on the finest resolution numerical experiment) could be examined. The disadvantage of the modon solution is that it is barotropic and thus does not test the baroclinic (variable density) aspects of the coupled model.

The modon results showed that, except for a small overestimate of the phase speed of the modon in all experiments, its structure and amplitude were quite well maintained in the fine domain while propagating there and when crossing the interface into the coarse region, at least for resolution differences of 3:1 and 5:1. At 7:1, the modon had some difficulty leaving the fine domain as it began to break up immediately upon entering the coarse region. Given a 5:1 resolution difference, the computational cost of the outer, coarse resolution model run compared to the inner, fine resolution one was 25%. Thus, this technique has considerable advantage over other techniques that try to extrapolate information from the interior of a fine resolution regional model to obtain boundary conditions for the proper exiting of such eddies. (In fact, the authors have not been able to achieve anything like comparable success using such extrapolation techniques for

the modon, which is a highly nonlinear and pathological eddy.)

The baroclinic vortex case shows quite comparable results as those for the modon. In general, factors of 3:1 and 5:1 in resolution were quite reasonably well behaved up until the baroclinic part of the solution crossed the interface between the two domains. Some error is found due to the rapidly propagating barotropic waves that rebound around the complete basin and reenter the fine domain. As the baroclinic eddy feature crosses the interface, there is also some underestimate of the temperature of the inflowing water, leading to a decrease in the maximum temperature near the boundary.

The present interaction between the coarse and fine grid regions does not conserve heat and momentum at the interface. The importance of flux conservation is complicated and likely to be related to the model application, time of integration, grid ratios, and subgridscale parameterizations. For the results presented in this study, the model performed quite well without exact flux conservation. It is not even clear that a conservative flux form of the fine grid boundary conditions would result in a better simulation since it was found that the solution degraded rather quickly as the eddy feature entered the coarse grid. Enforcing these coarse grid fluxes on the fine grid solution may actually propagate the erroneous coarse grid fields more quickly into the fine grid region. More analysis of the flux conservative form of the boundary conditions is needed before any conclusive comparison can be made, but the results found in this study indicate that nonconservative boundary conditions can be used for both baroclinic and barotropic problems of interest.

In general, the results shown here suggest that such coupled models are a very effective way in which to handle open boundaries of fine resolution numerical ocean models. At a reasonable cost in computer resources, a larger coarse resolution model may be added, with proper feedbacks, to properly handle the boundary conditions of the fine part of the domain. The other possibility, of using the outer coarse domain solution to force the fine domain with realistic flows [e.g., large scale seasonal changes in the circulation (see Holland and Vallis, 1990)], has not really been tested here, since only solutions initialized with eddy structures in the fine domain have been studied. There is no reason, however, for this coupled model system not to work equally well, as long as high resolution phenomena are not expected to enter or reenter the fine domain from the coarse one.

REFERENCES

Arakawa, A., and V. R. Lamb, 1977: Computational design of the basic dynamical processes of the UCLA general circulation model. *Methods in Computational Physics,* Vol. 17, J. Chang, Ed., Academic Press, 174–265.

Bryan, K., 1969: A numerical method for the study of the circulation of the world ocean. *J. Comput. Phys.*, **4,** 347–376.

——, and M. D. Cox, 1967: A numerical investigation of the oceanic general circulation. *Tellus,* **19,** 54–80.

Carton, J. A., 1984: Coastal circulation caused by an isolated storm. *J. Phys. Oceanogr.*, **14,** 114–124.

Cox, M., 1984: A primitive equation, three-dimensional model of the ocean. GFDL Ocean Group Tech. Rep. No. 1. GFDL, Princeton, NJ, 144 pp.

Engquist, B., and A. Majda, 1979: Radiation boundary conditions for acoustic and elastic wave calculations. *Commun. Pure Applied Math.*, **32,** 313–357.

Falkovich, A. I., 1986: Nested grid scheme for predicting isolated vortex movement in a barotropic model of the atmosphere. *Sov. Meteor. Hydrol.* **9,** 35–41.

Flierl, G. R., V. D. Larichev, J. C. McWilliams and G. M. Reznik, 1981: The dynamics of baroclinic and barotropic solitary eddies. *Dyn. Atmos. Oceans,* **5,** 1–41.

Holland, W. R., and G. Vallis, 1990: A high resolutional model of the California Current embedded into a basin-scale North Pacific circulation model.

Koss, W., 1971: Numerical integration experiments with variable resolution two-dimensional Cartesian grids using the box method. *Mon. Wea. Rev.*, **99,** 727–738.

Kurihara, Y., G. J. Tripoli and M. A. Bender, 1979: Design of a movable nested-mesh primitive equation model. *Mon. Wea. Rev.*, **107,** 239–249.

Ley, G. W., and R. L. Elsberry, 1976: Forecasts of typhoon Irma using a nested-grid model. *Mon. Wea. Rev.*, **104,** 1154–1161.

McWilliams, J. C., G. R. Flierl, V. D. Larichev and G. M. Reznik, 1981: Numerical studies of barotropic modons. *Dyn. Atmos. Oceans,* **5,** 219–238.

Orlanski, I., 1976: A simple boundary condition for unbounded hyperbolic flows. *J. Comput. Phys.*, **21,** 251–269.

Robinson, A. R., and L. J. Walstad, 1987: The Harvard open ocean model: calibration and application to dynamical process, forecasting, and data assimilation studies. *Appl. Num. Math.*, **3,** 89–131.

Ross, B. B., and I. Orlanski, 1982: The evolution of an observed cold front. Part I: Numerical simulation. *J. Atmos. Sci.*, **39,** 297–327.

Sobel, J. P., 1976: Nested grids in numerical weather prediction and an application to a mesoscale streak. PhD. thesis, Pennsylvania State University, 135 pp.

Spall, M. A., and A. R. Robinson, 1989: A new open-ocean hybrid coordinate primitive equation model. *Math. Comput.*, **31,** 241–269.

Yoon, J. H., and S. G. H. Philander, 1982: The generation of coastal undercurrents. *J. Ocean. Soc. Jpn.*, **38,** 215–224.

Zhang, D., H. Chang, N. L. Seaman, T. T. Warner and J. M. Fritsch, 1986: A two-way interacting nesting procedure with variable terrain resolution. *Mon. Wea. Rev.*, **114,** 1330–1339.